Environmental Engineering and Management Journal March 2021, Vol. 20, No. 3, 335-345
http://www.eemj.icpm.tuiasi.ro/; http://www.eemj.eu

"Gheorghe Asachi" Technical University of Iasi, Romania

HUMIC ACID REMOVAL FROM WATER BY SORPTION AND PHOTOCATALYSIS UNDER VIS IRRADIATION USING Fe_2O_3/SILICA NANOCOMPOSITE

Sorina Moțoc[1], Cătălin Ianasi[1], Anamaria Baciu[2], Claudia Delcioiu[2], Liviu Săcărescu[3], Ana-Maria Putz[1], Florica Manea[2]*

[1]*"Coriolan Dragulescu" Institute of Chemistry, Romanian Academy, 24 Mihai Viteazu Bvd., 300223 Timisoara, Romania;*
[2]*Department of Applied Chemsitry and Engineering of Inorganic Compounds and Environment, Politehnica University of Timisoara, 2 Victoriei Square, 300006 Timisoara, Romania*
[3]*Institute of Macromolecular Chemistry "Petru Poni", Aleea Grigore Ghica Voda 41A, 700487 Iasi, Romania*

Abstract

Hematite/silica nanocomposite (α-Fe_2O_3/SiO_2) was synthesized by sol-gel method at room temperature followed by thermal treatment through calcination at the temperature of 500° C selected based on thermo gravimetric analysis (TGA) and differential thermal analysis (DTA) results. The crystalline phases of α-Fe_2O_3 and SiO_2 were characterized by the correlation of X-ray diffraction (XRD) and Fourier transform infrared spectroscopy (FTIR) results. The composite average particle size values ranged between 10 and 22 nm were estimated through XRD and transmission electron microscopy (TEM). The composite exhibited a high capacity to remove humic acids (HA) from water, through the sorption and VIS irradiation-assisted photocatalysis processes. The heterogeneous structure of the composite was found by corroborating Brunauer–Emmett–Teller (BET) results with the HA sorption physical mechanism determined by Dubinin-Radushkevich isotherm model. A synergic effect regarding visible irradiation-assisted photocatalysis process using α-Fe_2O_3/SiO_2 was manifested for HA removal by comparison with the sorption and photolysis under VIS irradiation, which suggested a great potential for developing of a new nature-based inspired unitary processes for advanced treatment water for drinking purpose.

Key words: hematite/silica, humic acids, nanocomposite, water treatment

Received: June, 2020; Revised final: December, 2020; Accepted: January, 2021; Published in final edited form: March, 2021

1. Introduction

Water is the most essential compound on the earth for the human activities. Nowadays, most of the countries are facing drinking water problems and conditions are very severe especially in developing countries (Wankhade et al., 2013). Because the access to safe drinking water is the key to protect the public health, the clean water has become a basic need of all properly functioning societies.

Water pollution is increasing worldwide due to the rapid growth of industry, increasing human population, the domestic and agricultural activities, which lead to the life time threatening diseases (Tiwari et al., 2008).

Also, the environmental problems arise from the natural organic matter (NOM), e.g., humic acids (HA) and fulvic acids (Pansamut et al., 2013; Tiwari et al., 2008). Humic acids are the product of microbiological, chemical, and photochemical transformation of plants and animal residues. In fact, they are complex mixtures of components, which cannot be presented by any particular formula. Humic acids, with a complex nature composed of carboxylic, phenolic and carbonyl functional groups, cause a brown-yellow colour in water and are known to be the

* Author to whom all correspondence should be addressed: e-mail: florica.manea@upt.ro; Phone: +40256-403-071; Fax: +40256-403-069

precursors of carcinogenic halogenated compounds formed during the chlorination disinfection of drinking water. In a natural water system, HA is present in concentrations ranging from 0.1 to 200 mg L^{-1} (Joolaei et al., 2017; Liu et al., 2008).

It is well-known that several goals were set on the 2030 Agenda for Sustainable Development and the water quality improvement has received an increasing attention. Also, biomimetic process and materials have been searched to be developed for solar driven water purification though photocatalysis based on iron oxides that should be found in natural environment or can be synthesized and considered as nature-inspired process.

The traditional treatment methods for the removal and degradation of humic acids, such as: adsorption (Kim et al., 2016), coagulation (Barlokova and Ilavsky, 2012), ion-exchange (Brattebo et al., 1987), reverse osmosis membranes (Abdel-Karim et al., 2017), ozonation (Seredynska-Sobecka et al., 2006) and biological degradation (Seredynska-Sobecka et al., 2006), have their own limitations due to the cost and secondary pollution. However, photocatalytic oxidation (PCO) (Orha et al., 2016, 2017a, 2017b, 2018) as a clean production process has been reported to exhibit a significant advantage in treatment of humic acids.

In recent years, nanomaterial-based technologies have emerged as promising alternatives to current water treatment techniques at lower costs and high efficiencies that at the same time can meet the increasingly stringent water quality standards (Tiwari et al., 2008). Of particular interest among these nanomaterials are iron oxide nanoparticles considered as biomimetic material (Dave and Chopda, 2014; Ianasi et al., 2016; Nassar, 2012;). Nanoparticles of various polymorphic forms of iron oxides found their applications in such diverse areas as magnetic liquids (Ali et al., 2016), photocatalysis (Schwaminger et al., 2017), catalytic destruction of chlorinated organics (Hosseini, 2016), diagnostic imaging (Forge et al., 2008), and drug delivery (Forge et al., 2008).

α-Fe_2O_3 (hematite) form of the iron oxide is a promising material for photocatalytic applications owing to its narrow band gap of approximately 2.2 eV, chemical stability and nontoxicity, which absorbs light up to 600 nm, collects up to 40% of the solar spectrum energy, and it might be one of the cheapest and stable semiconductor materials (Kormann et al., 1989; Sugranez et al., 2015;). By absorbing visible light, the electrons of α-Fe_2O_3 are excited from the valence band to the conduction band, resulting excited electrons and the corresponding holes that can activate the surrounding chemical species and promote the chemical reactions (Kormann et al., 1989; Zhang et al., 2014). Various hematite based supported and/or nanocomposite materials including silica have been tested in particular for water and wastewater treatment considering a large ranges of inorganic and organic pollutants (Diagboya and Dikio, 2018; Lu et al., 2016; Xu et al., 2012). However, a study related the behavior of hematite-silica materials is required to elucidate some mechanistic and technical aspects for removal of HA considered as common matrix of drinking water sources.

The goal of this work is to investigate the potential application of α-Fe_2O_3/SiO_2 synthesized by sol-gel method for the advanced treatment of drinking water sources containing humic acids as natural organic matter using photocatalysis manifested under visible irradiation and/or sorption processes envisaging the future development of nature-inspired advanced drinking water treatment.

2. Experimental

2.1. Materials and composite materials preparation

All chemicals were commercially available: polyvinyl alcohol, Mw=72000 (PVA, degree of hydroxylation > 98%, Merck); $Si(OC_2H_5)_4$, tetraethyl orthosilicate (TEOS, 98 %, for synthesis, Merck); $Fe(C_5H_7O_2)_3$, [$Fe(acac)_3$], iron(III) acetylacetonate (99%, for synthesis, Merck); CH_3OH, methanol (99%, for analysis, Chimopar); HNO_3, nitric acid (65 %, for analysis, Merck). For the synthesis process, acid catalysed sol-gel route was used and one sample of $Fe(acac)_3$/silica/PVA hybrid xerogel nanocomposite was synthesized as previously published (Ianasi et al., 2016), but with different heat treatment in order to obtain pure hematite and by using a PVA polymer with a different molecular weight. The reactant mole ratio of TEOS: H_2O: PVA : $Fe(acac)_3$: MeOH : HNO_3 = 1 : 10 : $1.2*10^{-5}$: 0.20 : 18 : 0.01 was used, which means that 2.04 g of PVA (Mw= 72000) were dissolved in 90 mL of water at 85º C, by continuous stirring for 2 hours. The obtained solution was cooled down to room temperature and it was brought into a 100 mL volumetric flask. Also, 7.7 grams of iron (III) acetylacetonate were dissolved in 63.9 grams of methanol at 50 ºC by stirring for 15 minutes.

Acid solution (pH=1.5) was prepared by diluting 0.07 g HNO_3 (65%) in 15.1 g distilled water. The acid solution was then added to 23.7 g TEOS by stirring (30 minute) until the resulted sol was clear. Then, 5 g of 2% PVA solution was added by stirring for another 15 minutes. 69.3 g of the previously prepared methanolic solution of iron (III) acetylacetonate were subsequently added to the alkoxide-PVA hybrid sol sample and stirred for another 15 minutes. The composite sol sample was covered and left at room temperature in order to reach gelation. The gelation occurred after 4 days and during this process the resulting gel slightly cracked. After one month, the xerogel hybrid nanocomposite sample was thermally treated in air for 3 hours at 500 ºC temperature. The iron oxide was obtained by the thermal decomposition of the iron (III) acetylacetonate.

Humic acid (HA) was obtained from Sigma Aldrich, Switzerland, and 100 mg L^{-1} stock solution of HA was prepared by dissolving 0.1 g of HA in 1,000 mL of distilled water.

2.2. Characterization of the composite material

Thermogravimetric analysis was carried out between 25 and 500 °C in air flow at 5 °C/min heating rate, using an 851-LF 1100-Mettler Toledo apparatus. X-ray powder diffraction (XRD) measurements were performed at room temperature in transmission mode, over the 10°- 80° angular range (2θ), by means of a Panalytical X'Pert Pro MPD diffractometer, using Cu Kα radiation and X'Celerator detector. Fourier transform infrared spectroscopy (FTIR) measurements were performed on samples, pressed into pellets, prepared with KBr, using a JASCO FT/IR-4200 apparatus. The morphology and elemental analysis of iron oxide nanoparticles was examined by scanning electron microscopy (SEM) in conjunction with energy dispersive spectroscopy (EDAX) using a INSPECT S (FEI Company, Holland). Morphological characterization of the samples was carried out by transmission electron microscopy (TEM) by means of a High-Tech HT7700 transmission electron microscope (HITACHI), operated in high contrast mode at 100 kV accelerating voltage. The samples were prepared by drop casting from diluted dispersions of nanoparticles in ethanol on 300 meshes holey carbon coated copper grids (Ted Pella) and vacuum dried.

Textural properties of nanocomposites were analysed using nitrogen adsorption/desorption measurements at liquid nitrogen temperature (77 K) with a Quanta Chrome Nova 1200e apparatus. Prior each measurement, the materials were degassed for 3 hours in vacuum at 250 ºC.

2.3. Adsorption and photocatalysis experiments

All experiments regarding adsorption and photocatalysis processes were carried out under magnetic stirring at 20°C into a RS-1 photo-catalytic reactor (Heraeus, Germany), which consists of a submerged lamp surrounded by a quartz shield. Solutions of HA at different concentrations (prepared from an initial stock solution of 100 mg L^{-1}) were placed into the photoreactor and irradiated with a VIS light set between 460 and 510 nm, for 180 minutes. A system of water recirculation maintained a constant temperature of 20°C for the whole period of photocatalytic experiments.

The catalyst was placed into 300 mL HA solution. At regular time intervals of irradiation, samples were collected and filtered through a Milipore filter (pore size of 0.45 μm) in order to remove the α-Fe_2O_3/SiO_2 nanocomposite from the aqueous solution. The concentration of HA solutions was measured with a Varian Cary 100 UV-VIS spectrophotometer. The assessment of the photocatalysis performance was carried out as degradation efficiencies. The degradation efficiencies were determined based on the absorbance recorded at 254 nm. The pH of HA solution was adjusted by adding diluted H_2SO_4 and NaOH solutions (analytical grade), using an Inolab pH-meter. For all studied processes, The HA removal efficiency was calculated using the following equation (Eq. 1):

$$\textit{Removal efficiency } (\eta) = \frac{C_0 - C_t}{C_0} \times 100, \ (\%) \qquad (1)$$

where: C_0 and C_t are the concentrations of HA in aqueous solution in term of absorbance recorded at 254 nm (UV_{254}) at initial time and at any time t, respectively (mg L^{-1}).

For equilibrium study regarding HA adsorption on the composite material, Langmuir, Freundlich, and Dubinin-Radushkevich (D-R) models presented below were applied to assess the sorption isotherms.

The linear form of the Langmuir isotherm can be represented by the following (Eq. 2):

$$\frac{1}{q_e} = \left(\frac{1}{K_{Lqm}}\right) * \frac{1}{C_e} + \frac{1}{q_m} \qquad (2)$$

where: C_e is the equilibrium HA concentration at 30 min adsorption time (mg L^{-1}); q_m is the maximum adsorption capacity (mg g^{-1}); K_L is the Langmuir isotherm constant (L g^{-1}).

The Freundlich equation for a linear plot is described by the following (Eq. 3):

$$\ln q_e = \ln K_F + n \ln C_e \qquad (3)$$

where: K_F is the Freundlich constant (L g^{-1}); n is the heterogeneity factor.

The D-R equation is expresses in a linear form as (Eq. 4):

$$\ln q_e = \ln q_m - K_{DR\varepsilon^2} \qquad (4)$$

where q_m is the monolayer capacity (mol Kg^{-1}); ε is the Polanyi potential equal to RT ln (1+ 1/C_e); R is the gas constant (j mol^{-1} K^{-1}); T is the absolute temperature (K); K_{DR} is the constant of the adsorption energy (mol^2 $J K^{-1}$). The approach was usually applied to distinguish the physical and chemical adsorption of metal ions with its mean free energy, E per molecule of adsorbate (for removing a molecule from its location in the sorption space to the infinity) can be computed by the relationship (Eq. 5):

$$E = \frac{1}{\sqrt{2K_{DR}}} \qquad (5)$$

where: K_{DR} is denoted as the isotherm constant.

In order to determine some mechanism aspects regarding the sorption and photocatalysis processes, several models must be checked to find the optimum one. Two different kinetic models are used to fit the experimental data, *i.e.*, pseudo-first-order and pseudo-second-order kinetic model.

Pseudo-first-order kinetic model: The pseudo-first-order kinetics adsorption can be expressed in integrated form as (Eq. 6):

$$\ln(q_e - q_t) = \ln(q_e) - k_1 t \quad (6)$$

where: k_1 is the rate constant of adsorption (min^{-1}) and, q_t is the adsorption loading of α-Fe_2O_3/SiO_2 nanocomposite (mg g^{-1}) at time t (min);

Pseudo-second-order kinetic model: The pseudo-second-order kinetics is expressed as (Eq. 7):

$$\frac{t}{q_t} = \frac{1}{k_2 \cdot q_e^2} + \frac{t}{q_e} \quad (7)$$

where: k_2 is the rate constant of the pseudo-second-order adsorption kinetics (g mg^{-1} min^{-1}) and, q_e is the equilibrium adsorption capacity (mg g^{-1}).

3. Results and discussion

3.1. Structural and morphological characterization of α-Fe_2O_3/SiO_2 nanocomposite catalyst

The findings associated with formation and decomposition phase occurring during heat treatment of synthesized samples are in good agreement with thermo gravimetric analysis and differential thermal analysis (TGA and DTA) results (Fig. 1). The total weight loss was 43.15%, wt. and four distinct transformation steps were noticed. The first step in the 25°C-125°C domain was marked by endothermic effect resulted from the loss of the small molecules such as residual water and other solvents (Jitianu et al., 2006). The second step of 125 °C - 225 °C temperature interval corresponds to the loss of structural water (Kumar et al., 2000), removal of organics (Hamdy and Ismail, 1991) and mainly to the melting and the fractional decomposition of $Fe(acac)_3$ (Pal and Sharon, 2000).

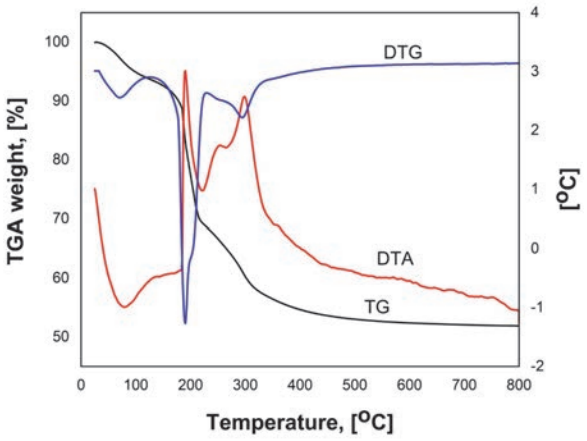

Fig. 1. Thermal curves (TGA, DTA, TG) of α-Fe_2O_3/SiO_2 nanocomposite in air atmosphere

In the case of hybrid nanocomposite samples, the DTA intensity changes and DTG maxima shift might be related to the PVA mass loss. In the third temperature interval, 225°C - 275°C the mass loss and exothermic effects were assigned to further hydrolysis or/and condensation (Brinker and Scherer, 1990) and dihydroxylation within the silica matrix, to the removal of organics (Hamdy and Ismail, 1991) and to the polymer chains cleavage (Sasipriya et al., 2013). This exothermic effect is due to the elimination of an acetylacetonate group from the metalo-organic compound and transformation in maghemite (γ-Fe_2O_3) (Pal and Sharon, 2000). The last thermal effect is assigned to the structural decomposition including the cleavage of C-C bonds of the polymer (Nakane et al., 1999; Sasipriya et al., 2013), further removal of organics (Hamdy and Ismail, 1991) and the condensation of OH groups in the silica matrix (Pal and Sharon, 2000). In this temperature interval, some parts of acetylacetonate group are still transforming to γ-Fe_2O_3 and also, hematite (α-Fe_2O_3) started to appear (Pal and Sharon, 2000). Another study emphasized that the pure PVA (molecular weight of 72000) disintegrates at 340 °C while in the composite material it is stable only up to 312 °C, because the introduced iron oxide affects the three-dimensional structure of the polymer by the weakening of the van der Waals interaction between the polymer chains (Kumar et al., 2000).

It can be seen that for all samples the main weight loss is encountered in the interval of temperature between 125-225° C, where $Fe(acac)_3$ is starting to transform and also, the highest amount of PVA is disintegrated. After 400 °C, the curve becomes parallel to the temperature axis, which emphasizes high stability of α-Fe_2O_3 nanoparticles. There is no signal associated with the thermal processes of α-Fe_2O_3 nanoparticles in the TGA curve, which confirmed that the crystallization and phase transition of α-Fe_2O_3 nanoparticles associated with them were finalized (Table 1).

Table 1. Results of the TGA curves for the anocomposites

Sample name	*Temperature interval*	*Weight loss, %*	*Type of process*	*Maximum peak, oC*
α-Fe_2O_3/ SiO_2 nanocomposite	25 - 125	6.21	endotherm	83
	125 - 225	18.28	exothermic	195
	225 - 275	4.47	exothermic	261
	275 - 800	14.19	exothermic	310

In order to investigate the crystal phase of hematite (α-Fe_2O_3) in the as-synthesized material, XRD analysis was carried out and the resulting diffraction patterns are shown in Fig. 2. The peaks positions and relative intensity correspond very well with the crystal structure of the hematite in according to ICDD PDF 01-079-0007. Besides the representative diffraction peak of the amorphous silica, the crystal planes of (104), (110), (113), (024), (116), and (300) are identified. The mean crystallites size obtained by Scherrer's equation, from the mean diffraction peaks, only, (104) and (110), is reported to be 22 nm.

The FTIR spectrum recorded for α-Fe_2O_3/ SiO_2 nanocomposite confirm the findings resulting from

XRD analysis and the major phases are α-Fe_2O_3 and SiO_2 (Fig. 3). The absorption bands presented in Table 2 match the Fe-O stretching of α-Fe_2O_3 and Si-O stretching and bending of Si-O_2.

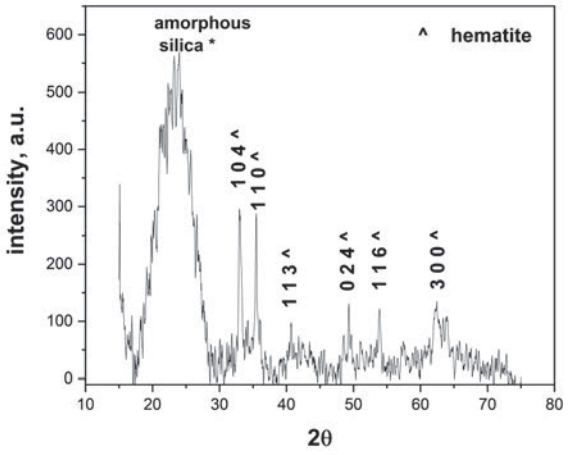

Fig. 2. XRD spectrum of synthesized nanocomposite material. Hematite peaks are indicated by ^ mark and amorphous silica by * mark

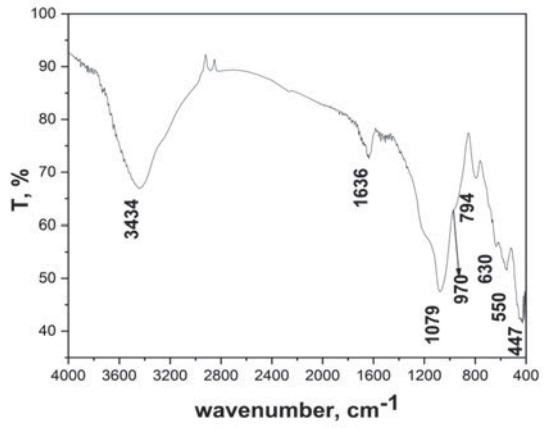

Fig. 3. FTIR spectrum of α-Fe_2O_3/ SiO_2 nanocomposite obtained after the thermal treatment at 500ºC

The IR band at 3434 cm^{-1} is due to the stretching vibration of H_2O molecules. Correspondingly, the IR band at 1636 cm^{-1} is due to the bending vibration of H_2O molecules (Music et al., 2011). Two absorptions bands around 550 and 447 cm^{-1} and the shoulder at around 630 cm^{-1} constitute a regular feature of the of the iron oxide samples, corresponded to Fe–O vibrations of Fe_2O_3 (Bepari et al., 2017; Rendon and Serna, 1981). The absorption bands at 1079 cm^{-1} have been reported to be the vibration of Si-O-Si asymmetric stretching (Pal and Sharon, 2000). The IR band at 800 cm^{-1} can be assigned to Si-O-Si symmetric stretching vibration (Music et al., 2011). The SEM image and EDX spectra of α-Fe_2O_3/SiO_2 nanocomposite annealed at 500 ºC is presented in Fig. 4. The estimation of the shape and average size of particles is almost impossible, because they are very small and not well defined, exhibiting a high agglomeration tendency.

Table 2. Assignments of infrared absorption bands (Ibrahim and Sani, 2014)

Bands (cm^{-1})	***Literature Assignment***	***α-Fe_2O_3/ SiO_2 nanocomposite assignment [this work]***
3580	Si-OH	-
3470	Fe-OH and H_2O (γOH stretch)	√
3360	Si-OH (γOH stretch)	-
1080	Si-O-Si (asymmetric stretch)	√
970	Si-O (stretch)	√
800	Si-O-Si (symmetric stretch)	√
680	Fe-O (asymmetric stretch)	√
460	O-Si-O (bend)	√
410	Fe-O (symmetric stretch)	-

However, a small fraction of the particles seems to exhibit a well-faceted, polyhedral shape and the other a rounded form of the particles. The qualitative composition of the composite given by EDAX results showed the presence of the Fe, Si, O besides the small residual carbon which can come from PVA decomposition, which is in agreement with FTIR results.

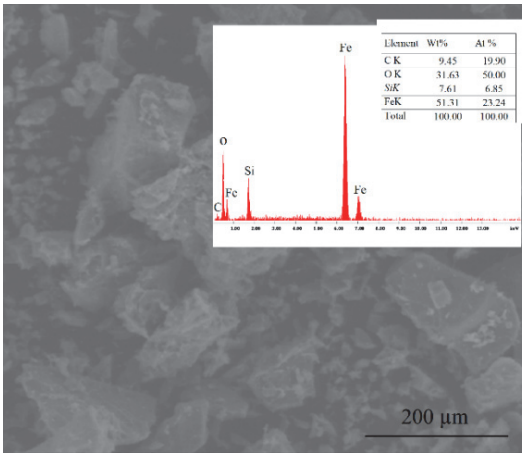

Fig. 4. SEM image of α-Fe_2O_3/SiO_2 nanocomposite annealed at 500ºC, inset: EDX spectrum of as-synthesized composite

In order to have a more realistic view on the size and morphology of as-synthesized composite, TEM investigations are required.

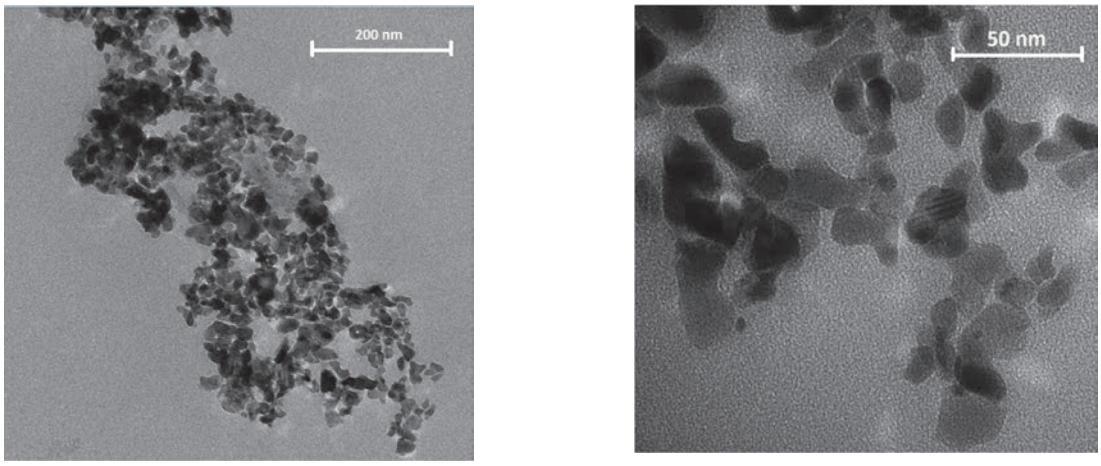

(a) (b)

Fig. 5. Transmission electron microscopy (TEM) at various magnifications: (a) 200 nm; (b) 50 nm

The individual particles exhibit sizes of 10-15 nm, were estimated from Figs. 5a and 5b, for the powders obtained after annealing at 500 °C. The particle sizes are smaller in comparison with the dimensions found by XRD measurememnts, but is is important to take into account that the dimensional features are observed in an incomparable smaller area compared with the sampling from the XRD measurements, which offers an objective image concerning the crystallite size the sample. The dimensional characteristics from each particle is evaluated in a direct way and automatically a mean value valid for the entire sample is provided (Nicola et al., 2020).

The distribution of the pore size (DFT) and N_2 (nitrogen) adsorption–desorption isotherms and of as-synthesized composite material are shown in Fig. 6. After IUPAC (Thommes et. al., 2015), analysing the sample a type Ib isotherm has been obtained, indicating the presence of micropores with larger widths.

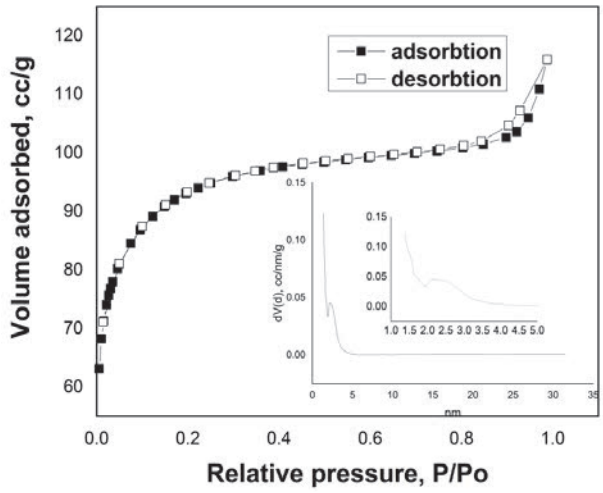

Fig. 6. N_2 adsorption-desorption isotherms of the α-Fe_2O_3/SiO_2 nanocomposite. Inset: Pore size distribution curves of the sample

The BET surface area has been found to be 350 m^2 g^{-1} with the total pore volumes of 0.179 cm^3 g^{-1}. By using the V-T method a micropore area of 246 m^2 g^{-1} has been obtained, indicating a high percent of microporosity. Using the DFT method we have obtained a bimodal pore size distribution with a value of 1.38 nm for the majority of sample representative for microporosity and a smaller part of 3.38 nm, which is representative for mesoporosity.

DRUV-VIS spectrum of the sample is shown in Fig. 7 and the absorption peaks in UV and VIS can be noticed with lower intensity for VIS region. The band gap energy (E_g) of the sample is determined by fitting the absorption data in according with Eq. (8) (Apopei et al., 2020):

$$\alpha h\nu = E_d (h\nu - E_g)^{1/2} \quad (8)$$

where: α - optical absorption coefficient, $h\nu$ - photon energy, Eg -direct band gap, E_d - constant.

The band gap value of 2.6 eV was determined by plotting $(\alpha h\nu)^2$ as a function of photon energy, and extrapolation the linear portion of the curve to absorption equal to zero, which is almost similar in comparison with simple α-Fe_2O_3 reported in the literature (Wu et al., 2014).

An important aspect in the sorption process is the surface charge of the material that depends on the pH and can be assessed through the ζ electrokinetic potential (presented in Table 3). Considering the material surface charge and the pollutant speciation function of pH, the material should exert the attraction or repulsion effect for the pollutant. It can be seen that the isoelectric point pH (zero charge surface) is close to 3.

Table 3. Zeta potential (ζ/mV) determined at the pH value of 3, 7 and 10

pH	3	7	9
ζ potential/mV	+6.50	-35.5	-51.20

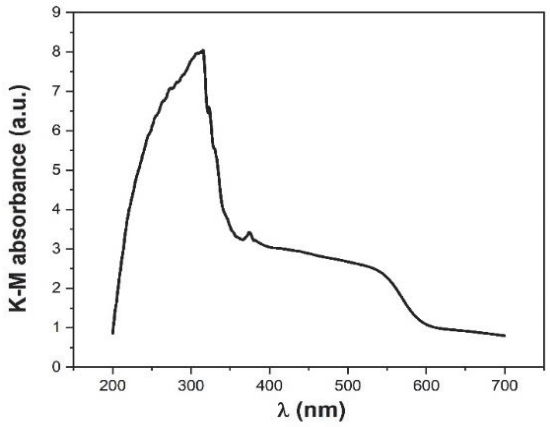

Fig. 7. DRUV-VIS absorbance spectra of α-Fe_2O_3/ SiO_2 nanocomposite

3.2. Composite application in humic acid removal from water by sorption and photocatalysis processes

The behaviour of α-Fe_2O_3/SiO_2 nanocomposite as sorbent and photocatalyst under VIS radiation was assessed comparatively for removal of humic acid (HA) from water. The sorption is considered as both self-standing unitary process and first stage of the photocatalysis. The effect of pH, initial HA concentrations and composite dose were considered to assess the HA removal efficiency.

3.2.1. Effect of the pH on sorption

It is well-known that pH is a critical controlling parameter in the sorption process because it may influence the HA speciation and the surface charges of the composite and implicit, the electrostatic forces. The time-evolution results of HA removal expressed as process efficiency (η) are presented in Fig. 8 for HA initial concentration of 25 mg*L^{-1} and composite dose of 0.5 g*L^{-1}. Taking into account the electrokinetic potential of the sample at various pHs, it is obviously that acidic pH favoured the sorption process of HA onto composite. pH range was chosen in related with the real water quality and taking into account that pH of 2 led to HA precipitation. Also, HA negative charge is enhanced at pH > 3 (Giasuddin et al., 2007) and composite became negatively charged at pH increasing, which means that on this pH range the electrostatic repulsive forces occurred, more intensively at higher pH. In addition, the stability of the composite is the best until to pH of 9 due to the solubility of the composite based on hematite and silica should increase in according with the literature data (Lazaro et al., 2017; Qin et al., 2015;). Based on these results, pH of 3 is considered as optimum and it will be chosen for future experiments.

3.2.2. Effect of the catalyst dose on removal efficiency

The influence of the catalyst dose was tested for 25 mg L^{-1} HA concentration and pH of 3. Fig. 9 presents the evolution of HA removal efficiency for composite doses of 0.1 and 0.5 g L^{-1}. Also, higher doses of nanocomposites were tested and a simultaneous sorption of HA occurred (the results are not shown here). It is obviously that increasing nanocomposite doses better HA removal efficiency was achieved through HA sorption onto the composite surface. However, the VIS irradiation effect imposes the limited doses to assure the light penetration through the aqueous solution.

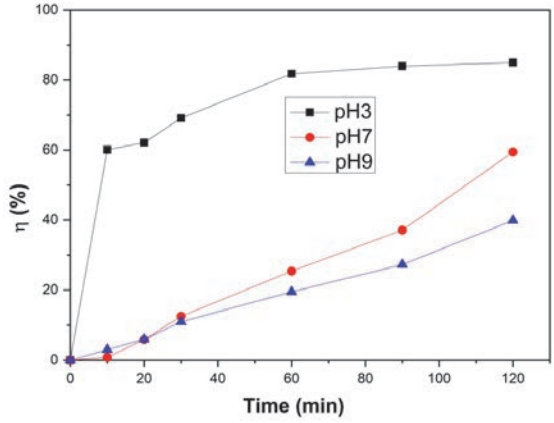

Fig. 8. Evolution of the humic acid removal efficiency using adsorption process using adsorbent initial dose of 0.5 g L^{-1} for HA initial concentration of 25 mg L^{-1} at different pH initial values: ■-3; ●-7; ▲-9

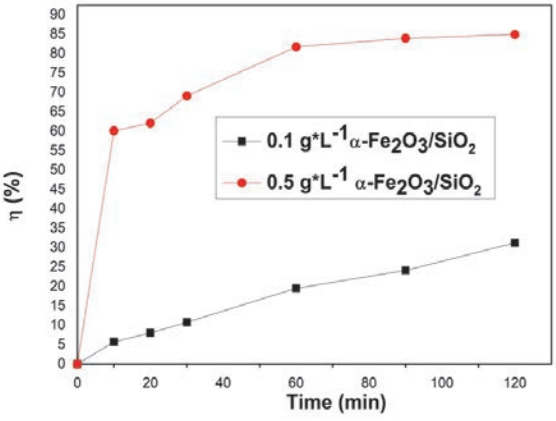

Fig. 9. Evolution of the humic acid removal efficiency of adsorption process under VIS irradiation for HA initial concentration of 25 mgL^{-1}, pH=3, using different α-Fe_2O_3/ SiO_2 nanocomposite doses: ■-0.1 g L^{-1}; ●-0.5 g L^{-1}

3.2.3. Effect of the initial HA concentration on sorption efficiency

Initial HA concentrations range gives information about the sorption process versatility and also, the thermodynamic and kinetics aspects should be elucidated. The sorption process efficiency increased at increasing initial HA concentration within the HA concentration range between 10 and 50 mg L^{-1} tested in this study, even if a lower reaction rate is found at higher HA concentration, which informed about a potential diffusion–controlled process (Fig. 10).

For the equilibrium study, Freundlich, Langmuir and D-R (Dubinin-Radushkevich) isotherm models were tested and only D-R fitted well the

experimental data with the correlation coefficient higher than 0.9 (Fig. 11).

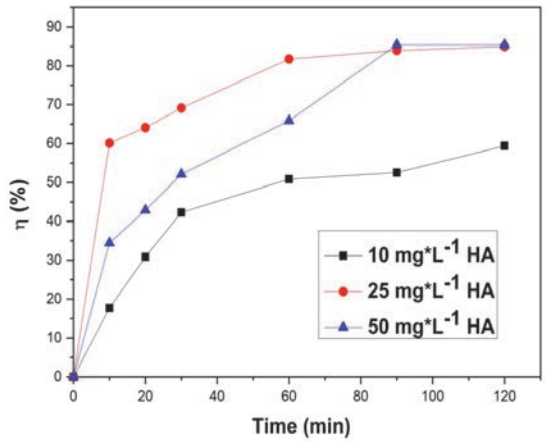

Fig. 10. Evolution of the humic acid removal efficiency using adsorption process using α-Fe_2O_3/ SiO_2 nanocomposite dose of 0.5 g*L^{-1} at pH=3, for the different initial HA concentrations: ■-10 mg*L^{-1} HA; ●-25 mg*L^{-1} HA; ▲-50 mg*L^{-1} HA

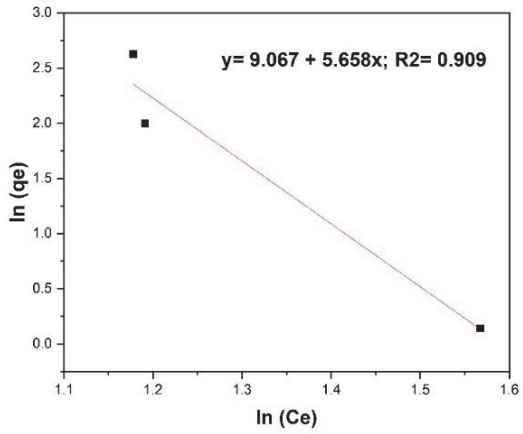

Fig. 11. The linearized form of the D-R isotherm

Table 4 gathered the results of the D-R sorption isotherm modelling and it can be highlighted that the obtained value of mean free energy, *E*, is 0.297 kJ mol^{-1} which is lower than 8 kJ mol^{-1}, informing about a physical sorption process mechanism (Ibrahim and Sani, 2014). A hydrophobic interaction and an entropic effect should be the major mechanisms by which HA are adsorbed onto composite in according with the literature data (Gu et al., 1994), probably due to that the presence of SiO_2 within the composite composition hinder the access of HA to hematite active sites and implicit, the potential ligand-exchange complexation process (Fu et al., 2005).

3.2.4. Comparative sorption and VIS irradiation photocatalysis testing

Considering the above-presented sorption results, photocatalytic process under VIS irradiation was tested for both composite doses of 0.1g L^{-1} and respectively 0.5 g*L^{-1} and the results are presented in Figs. 12 a-b. As we expected, the best effect of VIS result manifested for a composite dose of 0.1 g L^{-1}, higher dose (0.5 g L^{-1}) did not favour the photocatalyst process, probably due to the limitation of light penetration and implicit, the electron-hole formation did not occur.

Table 4. Sorption isotherm modeling results for HA onto α-Fe_2O_3/SiO_2 nanocomposite using Dubinin-Radushkevich model

Parameters	***Value***
E (KJ mol^{-1})	0.297
K_{DR} (mol^2 J K^{-1})	5.658
q_m (mol kg^{-1})	9.067
R^2	0.909

Pseudo-first- and pseudo-second-order kinetic models were tested for fitting the sorption and photocatalysis experimental data. The pseudo-second-order kinetic model (Table 5) fit very well the experimental data for photocatalysis and sorption of HA. The calculated q_e values agree very well with the experimental data, and the correlation coefficients for the pseudo-second-order kinetic model are higher than 0.90. It can be noticed the superiority of photocatalysis versus sorption process in relation to the process kinetics for both low and high nanocomposite doses, even if the sorption can be considered the first step of the overall photocatalytic process.

The photolysis process was applied for comparison to assess the contribution of each sorption and photolysis process and it can be seen that the overall photocatalysis process efficiency is higher than the sum of photolysis and sorption efficiencies after 20 minutes (Fig. 11), which confirm the effectivity of the photocatalytic process under VIS irradiation with composite dose of 0.1 g L^{-1}. Fig. 13 presents the comparative results obtained by applying photolysis, adsorption and photocatalysis for the treatment of water containing 25 mg L^{-1} HA, expressed by removal efficiency, determined using triplicates for each experiment.

Reusability of the material is checked by photocatalysis using 0.1 g L^{-1} α-Fe_2O_3/SiO_2 dose under VIS irradiation for 5 cycles, each cycle of 120 minutes. At the end of each cycle, the humic acid removal efficiency was checked and a diminution with 5 % was found after the fifth cycle, each denotes the self-cleaning capability of this material under VIS irradiation due to its photocatalytic activity and no other regeneration step is demand.

4. Conclusions

In this work, α-Fe_2O_3/SiO_2 was synthesized by sol-gel method at room temperature followed by thermal calcination at 500°C temperature for three hours. The formation and decomposition phases at each stage of the process were identified by TGA and DTA results and α-Fe_2O_3 and SiO_2 crystalline phases were proved by the correlation of XRD and FTIR.

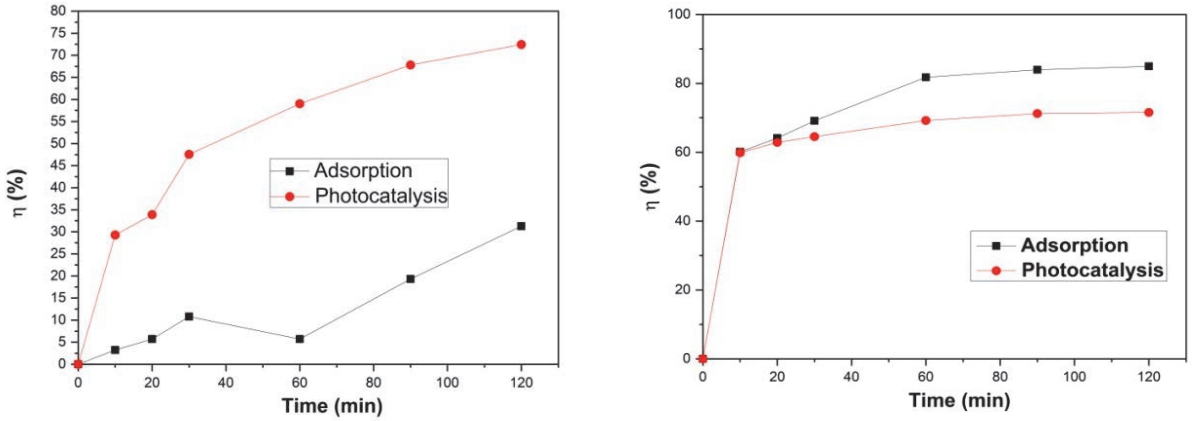

Fig. 12. Evolution of the HA removal efficiency for initial concentration of humic acid 25 mg L^{-1}, pH=3, by comparative adsorption process (■-Adsorption) vs. photocatalytic process under VIS irradiation (●-Photocatalysis) using α-Fe_2O_3/ SiO_2: 0.1 g L^{-1} (**a**) and 0.5 g L^{-1} (**b**)

Table 5. Pseudo-second order kinetics parameters for HA sorption and photocatalysis

Composite dose, g L^{-1}	*Parameters*	*HA concentration, 2 5mg·L^{-1}*	
		Adsorption	*Photocatalysis*
0.1	q_e(mg g^{-1})	10.07	14.19
	k_2(g·mg^{-1}·min^{-1})	0.0008	0.0027
	R^2	0.910	0.987
0.5	q_e(mg g^{-1})	17.89	18.73
	k_2(g·mg^{-1}·min^{-1})	0.0079	0.035
	R^2	0.998	0.999

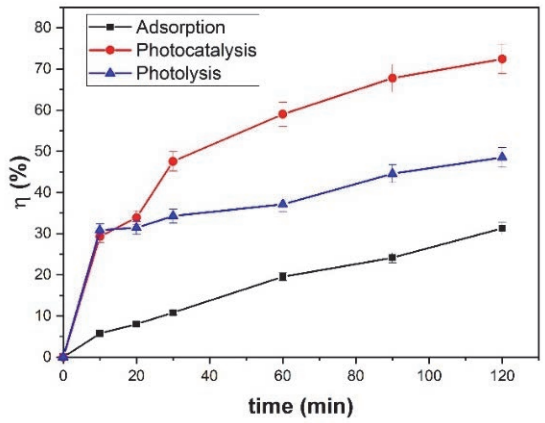

Fig. 13. Evolution of the humic acid removal efficiency by: ▲-Photolysis, ■-Adsorption and●-Photocatalysis using 0.1 g*L^{-1} α-Fe_2O_3/SiO_2 dose; Initial concentration of humic acid of 25 mg L^{-1}; pH=3

Even if the agglomeration tendency of the particles was noticed through SEM, however, the well-faceted, polyhedral shape for a small fraction of the particles and a rounded form for the other were evidenced. The average particle size values ranged from 10 to 22 nm were estimated through TEM and XRD. Specific surface area of 350 m^2/g and the total pore volumes of 0.179 cm^3g^{-1} were found from BET analysis, which confirmed microporous and mesoporous structure in the composite. α-Fe_2O_3/SiO_2 showed a high sorption capacity for humic acids removal from water. A physical mechanism of the sorption was elucidated from the results of the equilibrium study modeled by Dubinin-Radushkevich isotherm, which confirmed the heterogeneous structure of the composite. The visible irradiation-assisted photocatalysis process tested for HA removal suggested the solar irradiation based photocatalysis activity of the α-Fe_2O_3/SiO_2 proved by the band gap value of 2.6 eV determined by DRUV-VIS spectrum. These results offer a great potential for further investigations related in flow system and considering natural sand for developing new nature-based inspired unitary processes for advanced water treatment.

Acknowledgements

This work was supported by the Grant of the Romanian Ministry of Research and Innovation, CCCDI-UEFISCDI, project number 26PCCDI/01.03.2018, "Integrated and sustainable processes for environmental clean-up, wastewater reuse and waste valorization" (SUSTENVPRO), within PNCDI III.

References

Abdel-Karim A., Gad-Allah T.A., Badawy M.I., Khalil A.S.G., Ulbricht M., (2017), Removal of humic acid and chloroform from drinking water by using commercial nanofiltration and reverse osmosis membranes, *Desalination and Water Treatment*, **59**, 48-54.

Ali A., Zafar H., Zia M., Haq I., Phull A.R., Ali J.S., Hussain A., (2016), Synthesis, characterization, applications,

and challenges of iron oxide nanoparticles, *Nanotechnology, Science and Applications*, **9**, 49-67.

Apopei P., Orha C., Popescu M.I., Lazau C., Manea F, Catrinescu C., Teodosiu C., (2020), Diclofenac removal from water by photocatalysis- assisted filtrationusing activated carbon modified with N-doped TiO_2, *Process Safety and Environmental Protection*, **138**, 324-336.

Barlokova D., Ilavsky J., (2012), Removal of humic substances in water by coagulation, *Food and Environment Safety,* **9**, 31-36.

Bepari R.A., Bharali P., Das B.K., (2017), Controlled synthesis of α- and γ-Fe_2O_3 nanoparticles via thermolysis of PVA gels and studies on a-Fe_2O_3 catalyzed styrene epoxidation, *Journal of Saudi Chemical Society*, **21**, 170–178.

Brattebo H., Odegaard H., Halle O., (1987), Ion exchange for the removal of humic acids in water treatment, *Water Research*, **21**, 1045-1052.

Brinker C.J., Scherer G.W., (1990), *Sol-Gel Science, The Physics and Chemistry of Sol-Gel Processing*, Academic Press Inc., New York.

Dave P.N., Chopda L.V., (2014), Application of iron oxide nanomaterials for the removal of heavy metals, *Journal of Nanotechnology*, **1**, 1-14.

Diagboya P.N.E., Dikio E.D., (2018), Silica-based mesoporous materials; emerging designer adsorbents for aqueous pollutants removal and water treatment, *Microporous and Mesoporous Materials*, **266**, 252-267.

Forge S.L.D., Port M., Roch A., Robic C., Vander E.L., Muller R.N., (2008), Magnetic iron oxide nanoparticles: synthesis, stabilization, vectorization, physicochemical characterizations, and biological applications, *Chemical Reviews*, **108**, 2064-2110.

Fu H.B., Quan X., Chen S., Zhao H.M., Zhao Y.Z., (2005), Interaction of humic substances and hematite: FTIR study, *Journal of Environmental Sciences*, **17**, 43-47.

Giasuddin A.B.M., Kanel S.R., Choi H., (2007), Adsorption of humic acid onto nanoscale zerovalent iron and its effect on arsenic removal, *Environmental Science & Technology*, **41** , 2022–2027.

Gu B., Schmitt J., Chen Z., Liang L., McCarthy J.F., (1994), Adsorption and desorption of natural organic matter on iron oxide: mechanisms and models, *Environmental Science & Technology*, **28**, 38-46.

Hamdy M., Ismail A., (1991), Thermoanalytic study of metal acetylacetonates, *Journal of Analytical and Applied Pyrolysis*, **21**, 315–326.

Hosseini S.A., (2016), Catalytic oxidation of volatile organic compounds by using spinel mixed oxide catalyst- a review, *Advances in Ceramic Science and Engineering*, **5**, 1-10.

Ianasi C., Costisor O., Putz A.-M., Lazau R., Negrea A., Niznansky D., Sacarescu L., Savii C., (2016), Low temperature superparamagnetic nanocomposites obtained by Fe(acac)$_3$-SiO_2-PVA hybrid xerogel thermolysis, *Processing and Application of Ceramics*, **10**, 265-275.

Ibrahim M.B., Sani S., (2014), Comparative isotherms studies on adsorptive removal of Congo Red from wastewater by watermelon rinds and neem-tree leaves, *Open Journal of Physical Chemistry*, **4**, 139-146.

Jitianu A., Raileanu M., Crisan M., Predoi D., Jitianu M., Stanciu L., Zaharescu M., (2006), Fe_3O_4-SiO_2 nanocomposites obtained via alkoxide and colloidal route, *Journal of Sol-Gel Science and Technology*, **40**, 317-323.

Joolaei H., Vossoughi M., Rashidi Mehr Abadi A., Heravi A., (2017), Removal of humic acid from aqueous solution using photocatalytic reaction on perlite granules covered by nano particles, *Journal of Molecular Liquids*, **242**, 357-363.

Kim J.K, Jang D.G., Campos L.C., Jung Y.W., Kim J.-H., Joo J.C., (2016), Synergistic removal of humic acid in water by coupling adsorption and photocatalytic degradation using TiO_2/coconut shell powder composite, *Journal of Nanomaterials*, **1**, 1-10.

Kormann C., Bahnemann D.W., Hoffmann M. R., (1989), Environmental photochemistry: is iron oxide (hematite) an active photocatalyst? A comparative study: α-Fe_20, ZnO, TiO_2, *Journal of Photochemistry and Photobiology, A: Chemistry*, **48**, 161-169.

Kumar R.V., Koltypin Y., Cohen Y.S., Choen Y., Aurbach D., Palchik O., Felner I., Gedanken A., (2000), Preparation of amorphous magnetite nanoparticles embedded in polyvinyl alcohol using ultrasound radiation, *Journal of Materials Chemistry*, **10**, 1125-1129.

Lazaro A., Vilanova N., Barreto Torres L.D., Resoort G., Voets I.K., Brouwers H.J.H., (2017), Synthesis, polymerization, and assembly of nanosilica particles below the isoelectric point, *Langmuir*, **33**, 14618-14626.

Liu S., Lim M., Fabris R., Chow C., Chiang K., Drikas M., Amal R., (2008), Removal of humic acid using TiO_2 photocatalytic process – Fractionation and molecular weight characterisation studies, *Chemosphere*, **72**, 263-271.

Lu H., Wang J., Stoller M., Wang T., Bao Y., Hao H., (2016), An overview of nanomaterials for water and wastewater treatment, *Advances in Materials Science and Engineering*, **1**, 1-10.

Music S., Filipovic-Vincekovic N., Sekovanic L., (2011), Precipitation of amorphous SiO_2 particles and their properties, *Brazilian Journal of Chemical Engineering*, **28**, 89-94.

Nakane K., Yamashita T., Iwakura K., Suzuki, F., (1999), Properties and structure of poly(vinyl alcohol)/silica composites, *Journal of Applied Polymer Science*, **74**, 133-138.

Nassar N.N., (2012), *Iron Oxide Nanoadsorbents for Removal of Various Pollutants from Wastewater: An Overview*, In: *Application of Adsorbents for Water Pollution Control*, Bhatnagar A. (Ed.), Bentham Science Publisher, United Arab Emirates, 81-118.

Nicola R., Muntean S.-G., Nistor M.-A., Putz A.-M., Almásy L., Săcărescu L., (2020), Highly efficient and fast removal of colored pollutants from single and binary systems, using magnetic mesoporous silica, *Chemosphere*, **261**, 1-14.

Orha C., Manea F., Pop A., Bandas C., Lazau C., (2016), TiO_2-nanostructured carbon composite sorbent/photocatalyst for humic acid removal from water, *Desalination and Water Treatment*, **57**, 14178-4187.

Orha C., Lazau C., Ursu D., Manea F., (2017a), Effect of TIO_2 loading on powder-activated carbon in advanced drinking-water treatment, *WIT Transactions on Ecology and the Environment*, **216**, 203-211.

Orha C., Pode R., Manea F., Lazau C., Bandas C., (2017b), Titanium dioxide-modified activated carbon for advanced drinking water treatment, *Process Safety and Environmental Protection*, **108**, 26–33.

Orha C., Lazau C., Pode R., Manea F., (2018), Simultaneous removal of humic acid and arsenic (III) from drinking water using TiO_2-powdered activated carbon, *Journal of Environmental Protection and Ecology*, **19**, 39-47.

Pal B., Sharon M., (2000), Preparation of iron oxide thin film by metal organic deposition from Fe-acetylacetonate: a study of photocatalytic properties, *Thin Solid Films*, **379**, 83-88.

Pansamut G., Charinpanitkul T., Suriyawong A., (2013), Removal of humic acid by photocatalytic process: effect of light intensity, *Engineering Journal*, **17**, 25-32.

Qin X., Liu F., Wang G., Huang G., (2015), Adsorption of humic acid from aqueous solution by hematite: effects of pH and ionic strength, *Environmental Earth Sciences*, **73**, 4011-4017.

Rendon J.L., Serna C.J., (1981), Ir spectra of powder hematite: effects of particle size and shape, *Clay Minerals*, **16**, 375-381.

Sasipriya K., Suriyaprabha R., Prabu P., Rajendran V., (2013), Synthesis and characterisation of polymeric nanofibers poly(vinyl alcohol) and poly(vinyl alcohol)/silica using indigenous electrospinning set up, *Materials Research*, **16**, 824-830.

Schwaminger S.P., Surya R., Filser S., Wimmer A., Weigl F., Fraga-Garcia P., Berensmeier S., (2017), Formation of iron oxide nanoparticles for the photooxidation of water: alteration of finite size effects from ferrihydrite to hematite, *Scientific Reports*, **7**, 12791-12799.

Seredynska-Sobecka B., Tomaszewska M., Morawski A.W., (2006), Removal of humic acids by the ozonation–biofiltration process, *Desalination*, **198**, 265-273.

Sugranez R., Balbuena J., Cruz-Yusta M., Martin F., Morales J., Sanchez L., (2015), Efficient behaviour of hematite towards the photocatalytic degradation of NOx gases, *Applied Catalysis B: Environmental*, **165**, 529–536.

Tiwari D.K., Behari J., Sen P., (2008), Application of nanoparticles in waste water treatment, *World Applied Sciences Journal*, **3**, 417-433.

Thommes M., Kaneko K., Neimark A.V., Olivier J.P., Rodriguez-Reinoso F., Rouquerol J., Sing K.S.W., (2015), Physisorption of gases, with special reference to the evaluation of surface area and pore size distribution, *Pure and Applied Chemistry*, **87**, 1051-1069.

Wankhade A.V., Gaikwad G.S., Dhonde M.G., Khaty N. T., Thakare S.R., (2013), Removal of organic pollutant from water by heterogenous photocatalysis: a review, *Research Journal of Chemistry and Environment*, **17**, 84-94.

Wu W., Jiang C, Roy V.A.L., (2014), Recent progress in magnetic iron oxide-semiconductor composite nanomaterials as promising photocatalysts, *Nanoscale*, **7**, 38-58.

Xu P., Zeng G.M., Huang D.L., Feng C.L., Hu S., Zhao M.H., Lai C., Wei Z., Huang C., Xie G.X., Liu Z.F., (2012), Use of iron oxide nanomaterials in wastewater treatment: a review, *Science of the Total Environment*, **424**, 1-10.

Zhang X., Li H., Wang S., Fan F.-R.F., Bard A.J., (2014), Improvement of hematite as photocatalyst by doping with tantalum, *The Journal of Physical Chemistry C*, **118**, 16842-16850.